Cylindrical hot refractory anode vacuum arc (CHRAVA)

I. Camps (iD), S. Muhl, and Enrique Camps

View Online   Export Citation   CrossMark

ARTICLES YOU MAY BE INTERESTED IN

Record indoor magnetic field of 1200 T generated by electromagnetic flux-compression
Review of Scientific Instruments **89**, 095106 (2018); https://doi.org/10.1063/1.5044557

Note: A Laue crystal imager for high energy quasi-monochromatic x-ray
Review of Scientific Instruments **89**, 096106 (2018); https://doi.org/10.1063/1.5046108

Note: Multi-gap gas switch with low trigger-threshold voltage by mounting resistors and capacitors in parallel with switch gaps
Review of Scientific Instruments **89**, 096105 (2018); https://doi.org/10.1063/1.5026146

Cylindrical hot refractory anode vacuum arc (CHRAVA)

I. Camps,[1,2] S. Muhl,[1] and Enrique Camps[3]

[1]*Instituto de Investigaciones en Materiales, UNAM, Circuito Exterior s/n, C.U., A.P. 70-360, Ciudad de México, Mexico*
[2]*Instituto de Ciencias Físicas, UNAM, Ave. Universidad s/n, Col. Chamilpa, Cuernavaca, Morelos 62210, Mexico*
[3]*Instituto Nacional de Investigaciones Nucleares, Carretera México-Toluca S/N, Kilómetro 36.5. La Marquesa, Municipio de Ocoyoacac, Estado de México, Mexico*

We present a study of a novel vacuum arc deposition system composed of a water-cooled aluminum cathode and a hot refractory anode. The plasma of the arc system was diagnosed using a cylindrical electrostatic probe. It was found that the mean electron temperature was ~2 eV, the plasma density could be varied in the range of $0.5–6 \times 10^{16}$ m^{-3}, and the ion flux was between 0.06 and 0.35 A m^{-2}. Optical emission spectroscopy measurements showed the presence of emission lines corresponding to Al ı and Al ıı. The characterization of the coatings showed that the deposition rate varied from 0.8 to 4 nm/s and the surface roughness (Ra) of the films was as low as 25 nm. We demonstrated that it was possible to deposit films with low macroparticle densities, overcoming the principal disadvantage of the vacuum arc process. Measurements of the arc voltage and current were performed as a function of time and the applied magnetic field. The anode temperature was measured using a pyrometer through a ZnS window as a function of time and arc current, and the maximum value was 1800 °C with heating rates of up to 110 °C/s. *Published by AIP Publishing.* https://doi.org/10.1063/1.5025330

I. INTRODUCTION

The deposition techniques based on arc discharges have properties of particular interest; for instance, the classic cathodic vacuum arc can achieve high deposition rates (>10 nm/s).[1–3] Such high rates are of particular interest for certain industry sectors since they imply significant cost benefits. Today, these techniques are widely used to produce coatings for the automotive industry and decorative purposes,[4,5] as well as cutting tools.[6–8] Examples of such coatings include high hardness films with good adhesion and resistance to wear[9–11] and (TiAl)N, Ti(C,N), ZrN, CrN, and TiC.[12–14] A major limitation of the arc process for large area deposition is the inhomogeneity of the films. In part, this is due to the incorporation of non-vaporized molten material in the form of micron-size droplets, known as macroparticles (MPs).[15,16] In most vacuum arc systems, the anode plays a passive role and is only part of the electric circuit, but considering that approximately 1/2–2/3 of the arc power is dissipated as heat in the anode, several arrangements to increase the arc interaction between the electrodes have been proposed,[17] and among these are the Hot Anode Vacuum Arc (HAVA),[18] the Hot Refractory Anode Vacuum Arc (HRAVA),[2,19] and a newer version of the last system called Vacuum Arc with a Black-Body Assembly (VABBA).[20] For the HAVA, the material to be deposited is part of the anode, either as a rolled wire or in a crucible. When the anode is heated by the arc current, the material is evaporated without MPs. Ehrich *et al.* reported deposition rates up to 10 nm/s for Al and 3 nm/s for Ti.[21] The HRAVA version is a two part discharge; in the first, the cathodic arc expels the material from the cathode which, including the MPs, is deposited on a closely placed parallel refractory anode. The second part is that the arc heating of the anode causes the thermal evaporation of the deposited material without MPs,

and Beilis *et al.* reported deposition rates of 16–33 nm/s for Cu.[22] An important associated phenomenon is that the temperature of the anode can be sufficient to cause significant thermal emission of electrons so that the discharge is a combination of cathode and anode arcs.[2,23] The result is that the plasma between the close-spaced electrodes is very dense and can efficiently ionize the atoms evaporated from the anode. As for most vacuum arc systems, this allows the use of magnetic fields (MFs) to filter the ion flux and avoid the incorporation of MPs in the coating, as well as the possibility of the use of a bias voltage to coat substrates with complex shapes[17] (for example, the Filtered Vacuum Arc, FVA[24,25]). Anders[26] reported that vacuum arc systems can achieve plasma densities of 10^{26} m^{-3} near the cathode spot and up to 10^{18} m^{-3} near the substrate; for most metals, ion charge states of 2^+ and 3^+ have been observed and ion energies in the range of 20–120 eV for C and W, respectively.

In the present work, we describe a novel cylindrical vacuum arc discharge system and its operational parameters, as well as the characterization of the plasma and the deposited films as a function of the applied magnetic field strength and arc current. We call this system CHRAVA for Cylindrical Hot Refractory Anode Vacuum Arc.

II. EXPERIMENTAL SETUP

Figure 1 shows a schematic of the CHRAVA system. The cathode holder consisted of a water-cooled copper cylinder (4 cm internal diameter, 6 cm external diameter, and 5 cm long) with a 1 mm diameter insulated copper wire coil wound around the outside (15 layers and 50 turns/layer). The coil was connected to a 10 V/80 A power supply to generate a magnetic field of up to 20 Gauss, as measured with a Walker Scientific
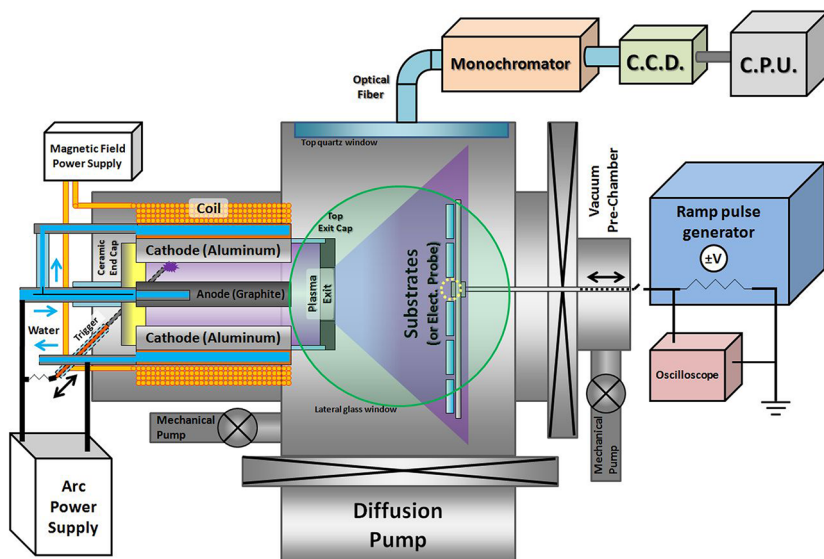
FIG. 1. Details of the cylindrical hot refractory anode vacuum arc. The position of the quartz window was in all the cases lateral to the plasma exit to avoid exposure. The position of the electrostatic probe is indicated with a dotted circle at the substrate position, and the ZnS window was in all cases frontal to the plasma exit to have a clear view-line between the pyrometer and the anode.

MG-40 Gauss-meter in the inter-electrode gap, which is the space to be occupied by the plasma. Both orientations of the magnetic field were used by simply reversing the polarity of the electrical connection. We define the positive field as having magnetic field lines along the axis of the cathode and toward the substrate.

The cathode was an aluminum tube, wall thickness 0.5 cm and 99.9% purity, machined to tightly fit inside the water-cooled copper holder. Graphite paste was used to ensure good electrical and thermal contact between the cathode and its holder. The anode was made from a 5 cm long 1 cm diameter cylindrical bar of high purity graphite, also connected to the water-cooling system on its base near the electrical feedthrough, and this was mounted concentrically in the cathode such that there was a 1 cm gap between the cathode and the anode. The cathode and the anode were mounted on a ceramic end-plate which was machined to avoid electrical connection between the electrodes even after deposition of aluminum. The electrical feedthrough and the connector to the anode were water cooled in order to avoid corrosion. To control and direct the plasma exit, an exit-cap was placed on the open-end of the cathode assembly; the idea was to allow the emission of ions and evaporated atoms but to block the expulsion of the macroparticles. This top cap was made of a graphite disc with a 1.5 cm central hole mounted on a 2 cm long glass tube fixed to the end of the cathode. The discharge was initiated by a mechanical trigger electrode, positioned diagonally to the axis of the anode-cathode assembly, but off-centre so that it only touched the inside surface of the cathode. However, it was found that after some operation time of the system, the Al thin film deposited on the ceramic end-cap was sufficient to be able to start the arc when the power supply was turned on, i.e., 70 V–300 A DC. The DC power supply used was a modified welding machine INFRA (Mexico) model MI 3-573 with a nominal exit of up to 600 A. The arc current was calculated from the voltage drop across a 20 mΩ resistor connected in the anode cable.

The temperature of the anode was measured using an Omega model OS523E pyrometer through a high IR-transparency ZnS *Cleartran* window. Given the arrangement of the system, the only direct view-path of the anode was through the top exit cap, so a special mount was made in order to place the ZnS window aligned in front of the anode; in Fig. 1 (not shown), this special mount was placed on the vacuum sample pre-chamber. This system was calibrated by measurements of an electrically heated graphite block connected to a K-type thermocouple, with the IR pyrometer viewing the graphite block through the ZnS window.

The substrates used were either Corning glass 7059 or Si (100), which were placed at a 10 cm distance in front of the exit of the plasma; the substrates were cleaned with a 5%-Extran solution, acetone, and ethanol, each for 15 min in an ultrasonic bath. A vacuum pre-chamber was implemented to allow sample changing without venting the arc vacuum chamber. In this study, the substrates were not heated, nor biased, and all experiments were carried out at an initial vacuum of 1.3×10^{-4} Pa; typically the pressure increased up to 6.7×10^{-4} Pa during the deposition process.

The thickness, deposition rates, and roughness, Ra, of the deposited films were determined using a Veeco Dektak 150 Profilometer with a stylus of 2.5 μm radius, and for the roughness, areas of 1 mm^2 were measured. For the thickness measurements, a simple line-mask with a permanent marker was made; this was then removed with acetone, leaving a measurable step. Since the deposition time varied between experiments, we only report the deposition rates. SEM images were obtained with a JEOL 76000 Field Emission at 15 kV. The plasma was analyzed with a cylindrical electrostatic probe made of a 5 mm long 0.25 mm diameter tungsten wire positioned where the substrates were placed, as indicated by the dotted circle in Fig. 1. These measurements were not simultaneous with the deposition experiments. The probe was connected to a 10 kHz triangular ramp pulse generator which polarized the probe from −25 to 5 V; these values ensured an adequate ion and electron collection. The data were collected using a Tektronix 320B Oscilloscope by measuring the voltage drop across a 1 kΩ resistor, and measurements of 128 ramps were averaged. The data were interpreted using the SONDA

software,[27] which uses the ionic region of the I–V characteristic[28] and supposes a non-collisional plasma to calculate the electron temperature and plasma density. The ion flux was calculated from the ion saturation current and the area of the probe exposed to the plasma; the degree of ionization of the deposition flux was estimated by comparing the measured thickness with the ion flux.

For the optical emission spectroscopy (OES) measurements, a quartz window was placed out of sight to the plasma exit on the cathode assembly to reduce exposure to the deposition flux. The emission was collected using an optical fibre connected to a Spectra Pro 500i Czerny-Turner type monochromator with a 1200 lines/mm grating. The light was detected using an ultra-fast intensified charge-coupled device (ICCD) Princeton Instruments 1024E and the data were analyzed using the WinSpec32 software.

III. RESULTS

A. Arc voltage and arc current

1. Arc trigger

Figure 1 shows the position of the mechanical trigger; when the electrical connection was interrupted, a "drawn arc" was created which produced the arc ignition. Nonetheless, often the discharge started at the moment the power supply was turned on; see 200 A arc discharge in Fig. 2. This was found to be caused by the formation of an Al thin film on the ceramic end-cap, which allowed electric contact between the electrodes. When the power supply was switched on, the current through this film evaporated it and started the arc discharge, making the system triggerless.

2. Arc operation

Figures 2 and 3 show typical temporal variations of the arc voltage and current. It can be seen that in the case of a 100 A, the initial open circuit voltage (∼70 V) provided by
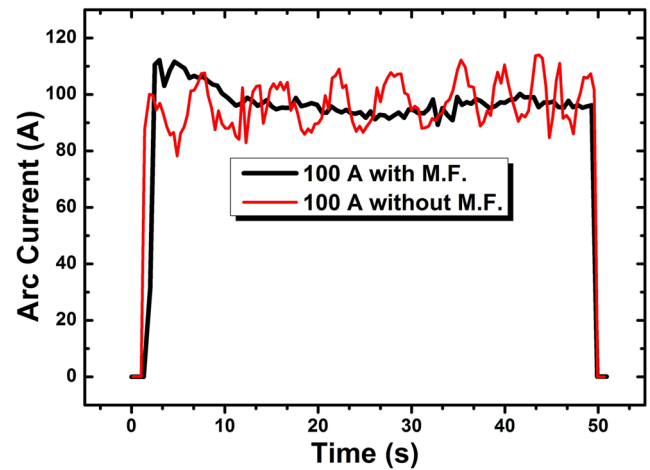
FIG. 3. Effect of the magnetic field (MF) on the arc current stability, for a 100 A arc.

the power supply dropped to close to 20 V once the arc was triggered. The arc voltage and current were almost constant during the ∼60 s experiment, except for the highest current of 200 A which increased slightly in time, probably related to an increase in conduction due to a temperature increase of the cathode.

The effect of the magnetic field on the deposition rate and roughness will be discussed later. It has been reported that in cathode arc systems, the presence of a magnetic field in the surroundings of the cathode surface affects the localization and trajectory of the cathode spots and localizes the erosion on the surface,[29] i.e., race-tracks. Furthermore, as can be seen in Fig. 3, the arc current in CHRAVA was more stable when a magnetic field was applied; moreover, the distribution of the cathode spots was increased over most of the electrode surface, hence allowing a more homogeneous erosion of the cathode.

B. Anode temperature

The heating rate of the anode is an important parameter to consider in such vacuum arc systems; in particular, for the CHRAVA, it is important that the anode be sufficiently hot to re-emit the material that has been deposited on its surface from the cathode arc. Figure 4 shows the temporal variation of the anode temperature for arc currents of 70, 100, and 200 A. It was observed that initially the heating was linear and increased with the arc current, as can be seen in the inset in Fig. 4. The maximum anode temperature depended on a combination of the arc current and duration of the experiment; for 70, 100, and 200 amperes, the maximum observed temperatures were 1400, 1500, and 1800 °C, respectively. For an arc current of 200 A, the heating rate was greater than 110 °C/s, and this meant that the melting point of aluminum deposited on the anode was reached in 10 s, and this is relevant in terms of the time it takes for the system to achieve the anodic mode, thus evaporating and emitting material from the anode surface.

C. Plasma diagnostics using Langmuir probe

Langmuir probe measurements were performed without the magnetic field and with the field in both the positive and
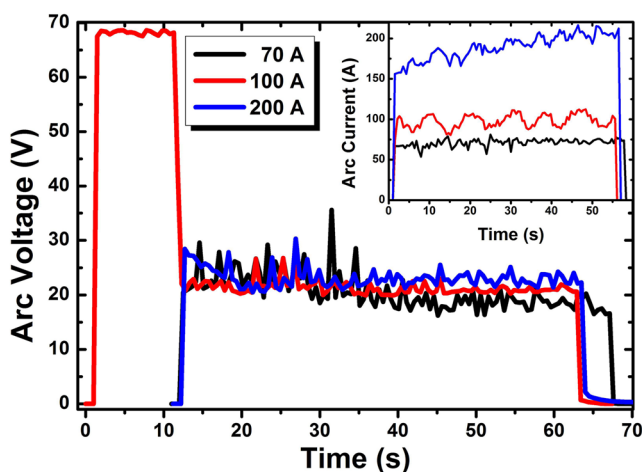

FIG. 2. Selected experiments of the CHRAVA system operation with output currents of 70, 100, and 200 A. For 100 A, the 70 V open circuit voltage of the power supply and the arc voltage of typically ∼20 V can be seen. The inset shows the temporal variation of the arc current, for each of the selected experiments.
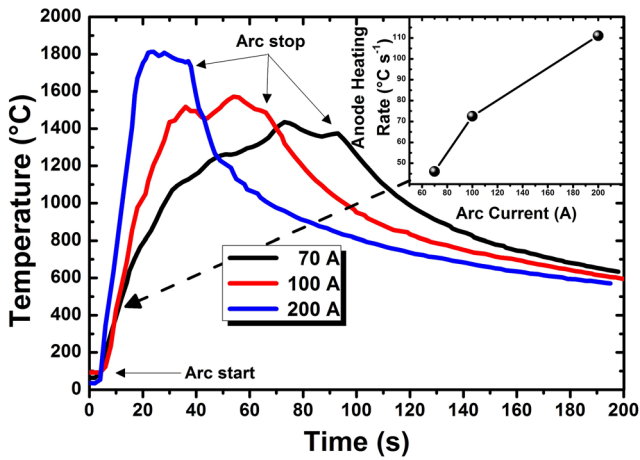
FIG. 4. The temperature of the anode during experiments using arc currents of 70, 100, and 200 A. The inset shows the value of the heating rate during the initial linear stage of the discharge.

FIG. 6. The plasma density for 70 and 100 A arc discharges, as a function of the magnetic field. (The lines connecting the dots are only visual guides and the error bars are the standard deviation of several measurements.)

negative orientations. Figure 5 shows the obtained values of T_e for arc currents of 70 and 100 A. As can be seen, there was no statistically significant variation as a function of either the magnetic field or the arc current and the average value was ~2 eV. This value is similar to that reported for plasmas produced in similar vacuum arcs systems[30,31] and materials.[32]

Figure 6 shows the variation of the plasma density as a function of the magnetic field for arc currents of 70 and 100 A. It can be seen that higher discharge currents produced a higher plasma density. The highest density was observed with no magnetic field, which was probably due to a confinement of the plasma within the cathode assembly due to the magnetic field and, therefore, a reduction of the electron flux to the probe at the substrate position.

From the ion saturation current from the $I-V$ characteristic and assuming that the ions were of single charge, we calculated the ion flux incident on the substrates. Figure 7 shows the ion flux as a function of the magnetic field for two values of the arc current. It can be seen that the flux tended to increase with the positive orientation of the magnetic field.

Using the ion flux data, it was possible to estimate the thickness deposited by the flow of the ions to the substrate and consequently the percentage of deposit due to the ions, h. Assuming that the density of aluminum films was that of the bulk, $\rho = 2.698$ g/cm^3, the sticking coefficient of the ions was one, and t was the deposition time in seconds, then

$$h = \frac{F_I t M_{Al}}{\rho N_A}, \qquad (1)$$

where F_I is the ion flux in ions/cm^2/s, M_{Al} is the gram molecular weight of aluminum, and N_A is Avogadro's number. Figure 8 presents, on the left vertical axis, both the film thickness measured using the profilometer (indicated as "Profilometry") and the calculated film thickness from the ion flux measurements (indicated as "Electrostatic Probe") versus the magnetic field, for 70 and 100 A arcs. The right axis represents the percentage ratio between the thicknesses obtained by the profilometer (T_{film}) over the calculated using the electrostatic probe (h), "% of Ion Deposit" (=$100 * h/T_{film}$). It can be seen
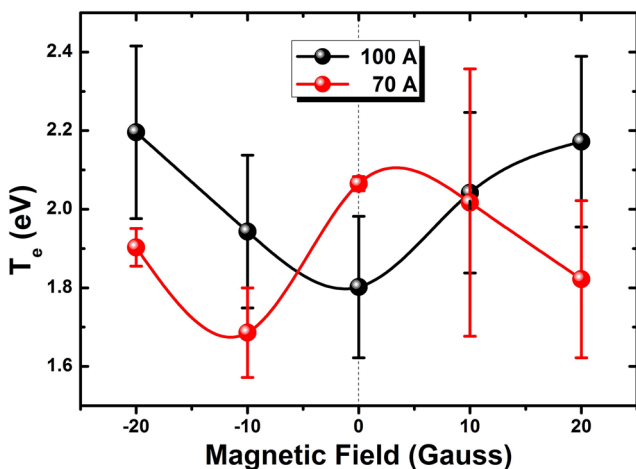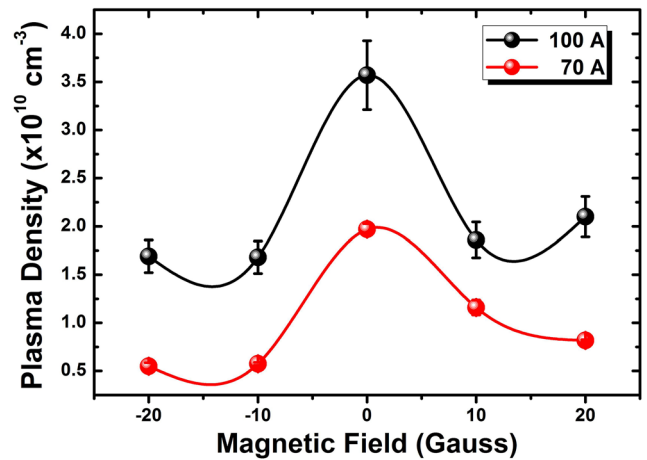

FIG. 5. The electron temperature for two arc currents, as a function of the magnetic field. (The lines connecting the dots are only visual guides and the error bars are the standard deviation of several measurements.)
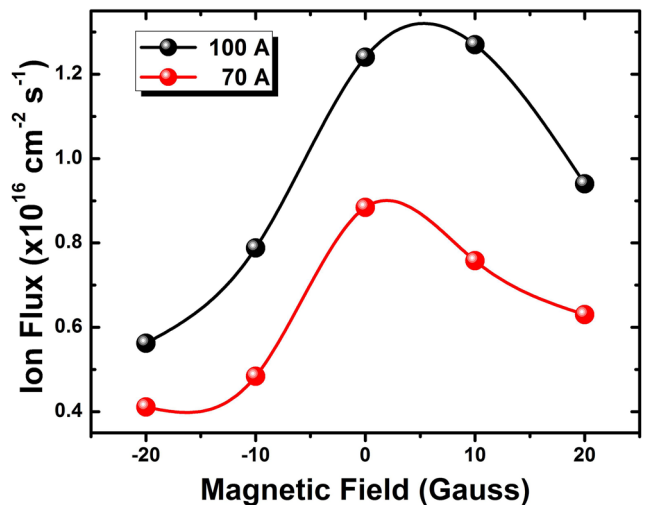

FIG. 7. The calculated ion flux as a function of the applied magnetic field for arc currents of 70 and 100 A. (The lines connecting the dots are only visual guides.)
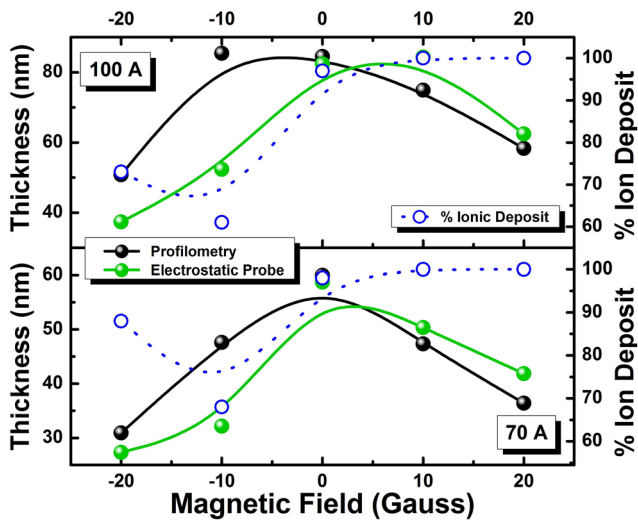
FIG. 8. The film thickness measured with the mechanical profilometer and the thickness calculated from the ion flux measured by the electrostatic probe. The right-hand side axis shows the percentage of the deposit due to the ion flux, assuming singly ionized Al ions and a sticking coefficient of unity.

FIG. 10. (a) The deposition rates and (b) surface roughness (Ra) as a function of the magnetic field. The roughness of the substrate was <13 nm.

that the positive orientation of the magnetic field is efficient for extracting ions toward the substrate; hence, the deposit was approximately 100% due to the ion flux.

D. Optical emission spectroscopy

During the discharge, the optical emission was monitored in two spectral regions: 270–310 nm and 370–410 nm. Using the NIST database, we identified the following characteristic wavelengths:[33]

- Al ɪ (neutral): 305.7, 308.2, 309.3, 344.5, 394.4, and 396.1 nm
- Al ɪɪ (1st ionization): 280.2, 281.6, 288.1, 358.7, and 390.1 nm

Figure 9 shows a sequence of typical emission spectra, with an acquisition interval of 1 s, for a 200 A arc without the magnetic field. The main emission lines were Al ɪ (394.4
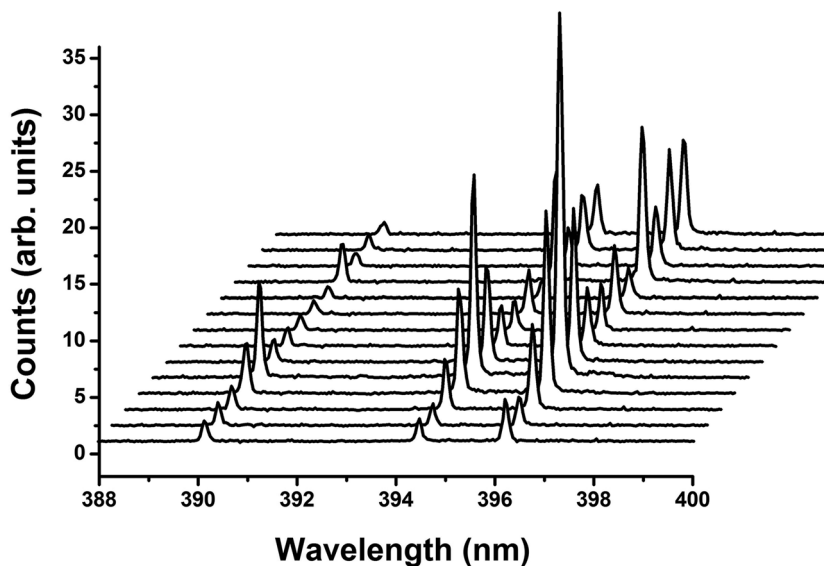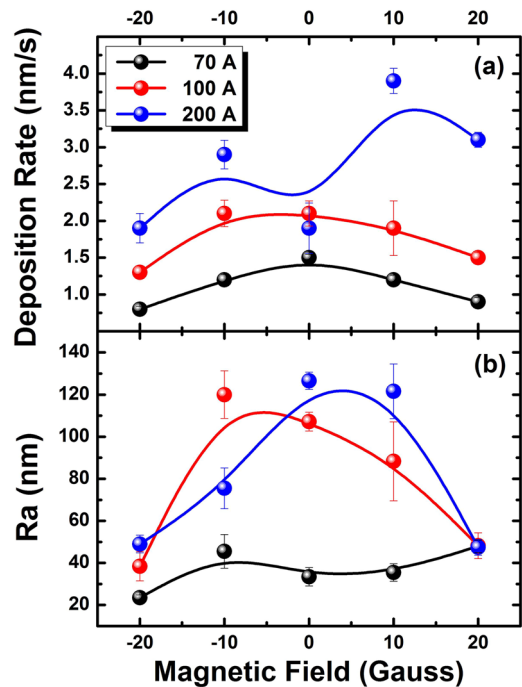
and 396.1 nm) and Al ɪɪ (390.1 nm). No significant changes in the spectra were observed during the discharge, and no signals were observed from carbon, oxygen, or nitrogen. The variation in the intensity of the lines was probably due to emission from different points of the cathode surface which were not completely in-line to the OES system.

E. Film deposition rate and surface roughness

As can be seen in Fig. 10(a), the deposition rate increased as the arc current was increased. For the 70 and 100 A arcs, the deposition rate decreased as the intensity of the magnetic field was increased, for both orientations of the field. This is in agreement with the plasma density results in that the magnetic

FIG. 9. The optical emission spectra for a 200 A arc. The emission lines correspond to Al I (394.4 and 396.1 nm) and Al ɪɪ (390.1 nm).
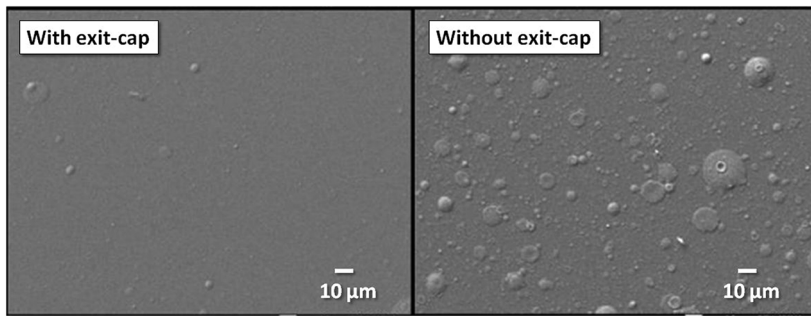
FIG. 11. SEM images showing MP coverage with and without the exit-cap.

field plays an important role in the extraction of the plasma due to magnetic confinement. For the highest arc current (200 A) and a positively oriented magnetic field, a deposition rate of 4 nm/s was obtained.

Figure 10(b) presents the values of the surface roughness of the deposited films. The 70 A arc resulted in films with a roughness of Ra ≈ 40 nm which did not vary with magnetic field. However, for the 100 and 200 A arcs, a magnetic field of ≤10 G produced a larger roughness of between 80 and 120 nm. At the highest magnetic fields of 20 G, in both orientations, the roughness dropped to values close to Ra ≈ 40 nm. All of the roughness values were greater than that of the substrate, Ra(Si) < 0.2 nm and Ra(Corning) ≈ 13 nm.

F. Film morphology and composition by SEM and EDX

Figure 11 presents SEM micrographs of samples prepared using a 200 A discharge with and without the exit-cap. The MP presence is evident in the case when no blockage was used. The exit-cap of the cathode was constructed on a trial-and-error basis to filter the MPs and reduce their incidence on the substrates. When the end-cap was in place, the homogeneity of the produced samples was greatly improved.

Finally, elemental analysis of the samples through energy dispersive x-ray (EDX) spectroscopy measurements in the SEM indicated that the samples were, within the experimental error of this technique, pure aluminum.

IV. CONCLUSIONS

In contrast to the HRAVA system[2,19] which generates a radial flux of atoms and ions useful for depositing films over large areas and closer to the newer version the VABBA system,[20,23] we present the CHRAVA system which can generate a beam of atoms and ions which can be directed at specific substrates. The inclusion of a magnetic field in the CHRAVA system is simple and it produced significant changes to the deposition flux; however, additional work is needed to fully understand the influence of the magnetic field. The arc current controlled the anode temperature, which increased rapidly to 2000 °C, and the deposition rate reached ~4 nm/s for arc discharges with 200 A. It was found that the system could produce a 100% Al ion flux for forming a deposit. Using an appropriate exit-cap, it was possible to deposit films with extremely low density of macroparticles.

[1] D. M. Sanders and A. Anders, "Review of cathodic arc deposition technology at the start of the new millennium," Surf. Coat. Technol. **133-134**, 78 (2000).

[2] I. I. Beilis and R. L. Boxman, "Metallic film deposition using a vacuum arc plasma source with a refractory anode," Surf. Coat. Technol. **204**, 865 (2009).

[3] P. J. Martin and D. R. Mckenzie, "Film growth," in *Handbook of Vacuum Arc Science and Technology*, edited by R. L. Boxman, P. J. Martin, and D. M. Sanders (Noyes, Park Ridge, NJ, 1995), Chap. 6, pp. 467–493.

[4] N. M. Mustapha and R. P. Howson, "Reactive filtered arc evaporation," Vacuum **60**, 361 (2001).

[5] B. B. Straumal, N. F. Vershinin, O. V. Gribkova, A. V. Kazakevich, A. Cantarero, J. Camacho, and A. Sanchez, "Vacuum arc deposition of decorative and protective coatings on the large-area glass and steel substrates," Uzbek J. Phys. **2**(1), 100 (2000).

[6] A. N. Panckow, J. Steffenhagen, B. Wegener, L. Dubner, and F. Lierath, "Application of a novel vacuum-arc ion-plating technology for the design of advanced wear resistant coatings," Surf. Coat. Technol. **138**, 71 (2001).

[7] Y. Tanaka, N. Ichimiya, Y. Onishi, and Y. Yamada, "Structure and properties of Al–Ti–Si–N coatings prepared by the cathodic arc ion plating method for high speed cutting applications," Surf. Coat. Technol. **146-147**, 215 (2001).

[8] J. Ramma, A. Neels, B. Widrig, M. Döbeli, L. de Abreu Vieira, A. Dommann, and H. Rudigier, "Correlation between target surface and layer nucleation in the synthesis of Al–Cr–O coatings deposited by reactive cathodic arc evaporation," Surf. Coat. Technol. **205**, 1356 (2010).

[9] J. Smolik, K. Zdunek, and B. Larisch, "Investigation of adhesion between component layers of a multi-layer coating TiC/Ti(C$_x$, N$_{1-x}$)/TiN by the scratch-test method," Vacuum **55**, 45 (1999).

[10] J. B. Wu, J. J. Chang, M. Y. Li, M. S. Leu, and A. K. Li, "Characterization of diamond-like carbon coatings prepared by pulsed bias cathodic vacuum arc deposition," Thin Solid Films **516**, 243 (2007).

[11] V. S. Sergevnin, I. V. Blinkov, D. S. Belov, A. O. Volkhonskii, A. Yu. Krupin, and A. V. Chernogor, "Hardness, adhesion strength, and tribological properties of adaptive nanostructured ion-plasma vacuum-arc coatings (Ti,Al)N–Mo$_2$N," Russ. J. Non-Ferrous Met. **57**(6), 572 (2016).

[12] P. J. Martin, R. P. Netterfield, T. J. Kinder, and L. Descotes, "Deposition of TiN, TiC, and TiO$_2$ films by filtered arc evaporation," Surf. Coat. Technol. **49**, 239 (1991).

[13] S. Anders, A. Anders, M. Rubin, Z. Wang, S. Raoux, F. Kong, and I. G. Brown, "Formation of metal oxides by cathodic arc deposition," Surf. Coat. Technol. **76**, 167 (1995).

[14] O. R. Monteiro, M. P. Delplancke-Ogletree, R. Y. Lo, R. Winand, and I. G. Brown, "Synthesis and characterization of thin films of WC$_x$ produced by mixing W and C plasma streams," Surf. Coat. Technol. **94-95**, 220 (1997).

[15] D. A. Karpov, "Cathodic arc sources and macroparticle filtering," Surf. Coat. Technol. **96**, 22 (1997).

[16] A. Anders, *Cathodic Arcs: From Fractal Spots to Energetic Condensation* (Springer-Verlag, New York, 2008).

[17] R. L. Boxman and V. N. Zhitomirsky, "Vacuum arc deposition devices," Rev. Sci. Instrum. **77**(2), 021101 (2006).

[18] H. Ehrich, "The anodic vacuum arc. I. Basic construction and phenomenology," J. Vac. Sci. Technol., A **6**, 134 (1988).

[19] I. I. Beilis, S. Goldsmith, and R. L. Boxman, "The hot refractory anode vacuum arc: A new plasma source for metallic film deposition," Surf. Coat. Technol. **133-134**, 91 (2000).

[20] I. I. Beilis, Y. Koulik, and R. L. Boxman, "Evolution of a plasma plume from a shower anode in a vacuum arc with a black-body electrode configuration," IEEE Trans. Plasma Sci. **39**(11), 2838 (2011).

[21] H. Ehrich, B. Hasse, K. G. Müller, and R. Schmidt, "The anodic vacuum arc. II. Experimental study of arc plasma," J. Vac. Sci. Technol., A **6**, 2499 (1988).

[22] I. I. Beilis, A. Shashurin, D. Arbilly, S. Goldsmith, and R. L. Boxman, "Copper film deposition by a hot refractory anode vacuum arc," Surf. Coat. Technol. **177-178**, 233 (2004).

[23] I. I. Beilis, Y. Koulik, and R. L. Boxman, "Cu ion current measurements in a vacuum arc with a black body electrode configuration," IEEE Trans. Plasma Sci. **41**(8), 1987 (2013).

[24] V. N. Zhitomirsky, L. Kaplan, R. L. Boxman, and S. Goldsmith, "Ion current distribution in a filtered vacuum arc deposition system," Surf. Coat. Technol. **76-77**, 190 (1995).

[25] R. L. Boxman, V. Zhitomirsky, B. Alterkop, E. Gidalevich, I. Beilis, M. Keidar, and S. Goldsmith, "Recent progress in filtered vacuum arc deposition," Surf. Coat. Technol. **86-87**, 243 (1996).

[26] A. Anders, "A review comparing cathodic arcs and high power impulse magnetron sputtering (HiPIMS)," Surf. Coat. Technol. **257**, 308 (2014).

[27] E. Camps, R. Ondarza, and G. Anguiano, "Programa de cómputo para el diagnóstico de plasmas con sondas eléctricas," Rev. Mex. Fis. **38**(5), 825 (1991).

[28] Yu. M. Kagan and V. I. Perel', "Probe methods in plasma research," Sov. Phys.-Usp. **6**(6), 767 (1964).

[29] B. Juettner *et al.*, "Cathode spots," in *Handbook of Vacuum Arc Science and Technology*, edited by R. L. Boxman, P. J. Martin, and D. M. Sanders (Noyes, Park Ridge, NJ, 1995), Chap. 3, pp. 73–281.

[30] S. Goldsmith, "The interelectrode plasma," in *Handbook of Vacuum Arc Science and Technology*, edited by R. L. Boxman, P. J. Martin, and D. M. Sanders (Noyes, Park Ridge, NJ, 1995), Chap. 4, pp. 282–307.

[31] I. I. Beilis, R. L. Boxman, and S. Goldsmith, "Radially expanding plasma parameters in a hot refractory anode vacuum arc," J. Appl. Phys. **88**, 6224 (2000).

[32] R. L. Boxman and S. Goldsmith, "Excited-state densities in a multicathode-spot Al vacuum arc. I. Spectroscopic measurements," J. Appl. Phys. **51**, 3644 (1980).

[33] Yu. Ralchenko *et al.*, *NIST Atomic Spectra Database (Version 4.1.0)*, Online (National Institute of Standards and Technology, Gaithersburg, MD, 2011), http://physics.nist.gov/asd.